

# Linked cluster expansions for open quantum systems on a lattice

Alberto Biella,<sup>1</sup> Jiasen Jin,<sup>2</sup> Oscar Viyuela,<sup>3,4</sup> Cristiano Ciuti,<sup>1</sup> Rosario Fazio,<sup>5,6</sup> and Davide Rossini<sup>7</sup>

<sup>1</sup>*Université Paris Diderot, Sorbonne Paris Cité, Laboratoire Matériaux et Phénomènes Quantiques, CNRS-UMR7162, 75013 Paris, France*

<sup>2</sup>*School of Physics, Dalian University of Technology, 116024 Dalian, China*

<sup>3</sup>*Department of Physics, Massachusetts Institute of Technology, Cambridge, MA 02139, USA*

<sup>4</sup>*Department of Physics, Harvard University, Cambridge, MA 02318, USA*

<sup>5</sup>*ICTP, Strada Costiera 11, I-34151 Trieste, Italy*

<sup>6</sup>*NEST, Scuola Normale Superiore and Istituto Nanoscienze-CNR, I-56126 Pisa, Italy*

<sup>7</sup>*Dipartimento di Fisica, Università di Pisa and INFN, Largo Pontecorvo 3, I-56127 Pisa, Italy*

(Dated: December 14, 2024)

We propose a generalization of the linked-cluster expansions to study driven-dissipative quantum lattice models, directly accessing the thermodynamic limit of the system. Our method leads to the evaluation of the desired extensive property onto small connected clusters of a given size and topology. We first test this approach on the isotropic spin-1/2 Hamiltonian in two dimensions, where each spin is coupled to an independent environment that induces incoherent spin flips. Then we apply it to the study of an anisotropic model displaying a dissipative phase transition from a magnetically ordered to a disordered phase. By means of a Padé analysis on the series expansions for the average magnetization, we provide a viable route to locate the phase transition and to extrapolate the critical exponent for the magnetic susceptibility.

## I. INTRODUCTION

The recent technological breakthroughs in the manipulation of many-body systems coupled to an external bath are setting the ground for a careful testing of a new wealth of physical phenomena in the quantum realm<sup>1–3</sup>. Specifically, several promising experimental platforms aimed at investigating the scenario emerging from driven-dissipative quantum many-body systems have been recently proposed and realized in the lab. The most remarkable ones are atomic and molecular optical systems through the use of Rydberg atoms, trapped ions or atomic ensembles coupled to a condensate reservoir<sup>4</sup>, arrays of coupled QED cavities<sup>5</sup>, or coupled optomechanical resonators<sup>6</sup>. These implementations are scalable enough to enable the construction of tunable and interacting artificial lattice structures with hundreds of sites.

The coupling between different unit cells can give rise to a plethora of cooperative phenomena determined by the interplay of on-site interactions, nonlocal (typically nearest-neighbor) processes, and dissipation<sup>7–11</sup>. Recently, a large body of theoretical works has been devoted to the investigation of the collective behavior emerging in dynamical response<sup>12</sup>, many-body spectroscopy<sup>13–15</sup>, transport<sup>16–20</sup>, as well as stationary properties. In the latter context, a careful engineering of the coupling between the system and the environment can stabilize interesting many-body phases in the steady state<sup>21,22</sup>. The phase-diagram of such lattice systems has been predicted to be incredibly rich<sup>23–30</sup> and can display spontaneous ordering associated with the breaking of a discrete<sup>31–33</sup> or continuous symmetry<sup>34,35</sup> possessed by the model. Recently, the critical behavior emerging at the onset of phase transitions started to be investigated by means of different analytical and numerical approaches<sup>36–39</sup>.

Theoretically, while at equilibrium we have reached a

fairly good understanding of several aspects of the many-body problem under the framework of textbook statistical mechanics, this is no longer the case for quantum systems coupled to some external bath. In such case, we are indeed facing an inherently out-of-equilibrium situation, where the Hamiltonian of the system  $\hat{H}$  is no longer capable to describe it in its whole complexity, and the environmental coupling needs to be accounted for and suitably modeled. Due to the intrinsic difficulty of the problem, a number of approximations are usually considered, which assume a weak system-bath coupling, neglect memory effects in the bath, and discard fast oscillating terms. In most of the experimental situations with photonic lattices, these assumptions are typically met<sup>5,40</sup>.

As a result, in many cases of relevance, the coupling to the environment leads to a Markovian dynamics of the system's density matrix  $\rho$ , according to a master equation in the Lindblad form<sup>41</sup>:

$$\partial_t \rho = \mathbb{L}[\rho] = -i[\hat{H}, \rho] + \mathbb{D}[\rho], \quad (1)$$

where  $\mathbb{L}$  denotes the so called Liouvillian superoperator (we will work in units of  $\hbar = 1$ ). While the commutator in the r.h.s. of Eq. (1) accounts for the unitary part of the dynamics, the dissipative processes are ruled by

$$\mathbb{D}[\rho] = \sum_j \left[ \hat{L}_j \rho \hat{L}_j^\dagger - \frac{1}{2} \{ \hat{L}_j^\dagger \hat{L}_j, \rho \} \right], \quad (2)$$

where  $\hat{L}_j$  are the jump operators. The master equation (1) covers a pivotal role in the treatment of open quantum systems, since it represents the most general completely-positive trace preserving dynamical semigroup<sup>42</sup>. In the following we will restrict our attention to it, and specifically address the steady-state (long-time limit) solution  $\rho_{\text{SS}} = \lim_{t \rightarrow \infty} \exp(\mathbb{L}t) \rho(0)$  (and thus  $\partial_t \rho_{\text{SS}} = 0$ ) in situations where the steady state is guaranteed to be unique<sup>43</sup>.

Solving the long-time dynamics ruled by Eq. (1) for a many-body system is a formidable, yet important, task. Indeed contrary to equilibrium situations, the effect of short-range correlations can be dramatic in a driven-dissipative context, and thus they deserve an accurate treatment through the (in principle) full many-body problem. Exact solutions are restricted to very limited classes of systems, which are typically represented by quadratic forms in the field operators and specific jump terms<sup>44</sup>. A number of viable routes have been thus proposed, in the recent few years. Under certain hypotheses, analytic approaches such as perturbation theory<sup>45</sup> or renormalization-group techniques based on the Keldysh formalism<sup>9,46</sup> are possible. However, their limited regime of validity calls for more general numerical methods which do not suffer these limitations.

From a computational point of view, the main difficulty resides in the exponential growth of the many-body Hilbert space with the number  $N$  of lattice sites. Moreover, the non-Hermitian Liouvillian superoperator  $\mathbb{L}$  acts on the space of density matrices (whose dimension is the square of the corresponding Hilbert space dimension), and its spectral properties are generally much more difficult to be addressed than the low-lying eigenstates of a Hamiltonian system. The difficulty remains even for the fixed point of the dynamics  $\rho_{\text{SS}}$ , that is the density matrix associated with the zero-eigenvalue of  $\mathbb{L}$ .

While in one dimension tensor-network approaches based on a straightforward generalization of matrix product states to operators can be effective<sup>47–49</sup> and alternative strategies have been proposed in order to improve their performances<sup>50–52</sup>, going to higher dimensions is much harder. Numerical strategies specifically suited for this purpose have been recently put forward, including cluster mean-field<sup>53</sup>, correlated variational Ansätze<sup>54,55</sup>, truncated correlation hierarchy schemes<sup>56</sup>, corner-space renormalization methods<sup>57</sup>, and even two-dimensional tensor-network structures<sup>58</sup>. Each of such methods presents advantages and limitations, and typically performs better on specific regimes.

In this paper we will adapt a class of techniques that, in the past, has revealed to be extremely useful and versatile in the study of thermal and quantum phase transitions<sup>59</sup>. The key idea consists in computing extensive properties of lattice systems in the thermodynamic limit, out of certain numerical series expansions. The method, dubbed linked-cluster expansion (LCE), sums over different contributions associated to clusters of physical sites. In combination with perturbation theories, LCEs have already proved their worth in the context of equilibrium statistical mechanics, both in classical and quantum systems (see Ref. 59 and references therein). Their predictive power lies beyond the range of validity of the perturbation expansion: using established tools for the analysis of truncated series<sup>60</sup>, it has been possible to study equilibrium quantum phase transitions, and extract critical exponents. Here we focus on numerical linked-cluster expansions (NLCEs), where the  $k$ -th order contribution

in the LCE is obtained by means of exact diagonalization techniques on finite-size clusters with  $k$  sites<sup>61</sup>. The NLCE has been successfully employed in order to evaluate static properties at zero and finite temperature<sup>62</sup>, as well as to study the long-time dynamics and thermalization in out-of-equilibrium closed systems<sup>63,64</sup>. Moreover it has also revealed its flexibility in combination with other numerical methods that can be used to address finite-size clusters, such as density-matrix renormalization group algorithms<sup>65</sup>. Nonetheless, to the best of our knowledge, it has never been applied in the context of open quantum systems.

Here we see NLCE at work in an interacting two-dimensional spin-1/2 model with incoherent spin relaxation<sup>32</sup>, which is believed to exhibit a rich phase diagram, and represents a testing ground for strongly correlated open quantum systems<sup>39,53,58</sup>. We will test our method both far from critical points, and in the proximity of a phase transition: in the first case NLCE allows us to accurately compute the value of the magnetization, while in the latter we are able to estimate the critical point as well as the critical exponent  $\gamma$  for the divergent susceptibility.

The paper is organized as follows. In Sec. II we introduce our NLCE method and discuss how it can be applied to the study of the steady-state of a Markovian Lindblad master equation. The NLCE is then benchmarked in a dissipative two-dimensional spin-1/2 XYZ model (Sec. III). By properly tuning the coupling constants of the Hamiltonian, we are able to study steady-state properties far away from any phase boundary (Sec. III A), and a more interesting scenario exhibiting a quantum phase transition from a paramagnetic to a ferromagnetic phase (Sec. III B). In the latter case we discuss a simple strategy (based on the Padé analysis of the expansion) in order to locate the critical point and to extrapolate the critical exponent  $\gamma$ . Finally, Sec. IV is devoted to the conclusions.

## II. LINKED-CLUSTER METHOD

We start with a presentation of the NLCE formalism<sup>61</sup>, unveiling its natural applicability to the study of driven-dissipative quantum systems whose dynamics is governed by a Lindblad master equation. We follow an approach that is routinely employed in series expansions for lattice models, such as high-temperature classical expansions<sup>59</sup>. Since we are interested in the steady-state properties of the system, our target objects will be the expectation values of generic extensive observables  $\hat{\mathcal{O}}$  onto the asymptotic long-time limit solution  $\rho_{\text{SS}}$  of the master equation:  $\mathcal{O} = \text{Tr}[\hat{\mathcal{O}}\rho_{\text{SS}}]$ . We stress that there are no restrictions in the limits of applicability of this approach to different scenarios, which can be straightforwardly extended to the case of generic non-Markovian master equations and/or non-equilibrium states  $\rho(t)$ .

Let us first write the Liouvillian operator  $\mathbb{L}$  as a sum of local terms  $\mathbb{L}_k$ , each of them supposedly acting on

few neighbouring sites. For the sake of simplicity and without loss of generality, each term  $\mathbb{L}_k$  only couples two neighboring sites:

$$\mathbb{L} = \sum_k \alpha_k \mathbb{L}_k = \sum_{\langle i,j \rangle} \alpha_{ij} \mathbb{L}_{ij}, \quad (3)$$

where  $\alpha_{ij}$  denotes the local coupling strength, and the index  $k = (i, j)$  is a short-hand notation for the couple of  $i$ - $j$  sites. The terms of  $\mathbb{L}$  acting exclusively on the  $i$ th site can be arbitrary absorbed in the terms of the sum such that  $i \in k$ . The observable  $\mathcal{O}$  can be always arranged in a multivariable expansion in powers of  $\alpha_k$ :

$$\mathcal{O}(\{\alpha_k\}) = \sum_{\{n_k\}} \mathcal{O}_{\{n_k\}} \prod_k \alpha_k^{n_k} \quad (4)$$

where  $n_k$  runs over all non-negative integers for each  $k$ . The expansion (4) can be reorganized in clusters:

$$\mathcal{O} = \sum_c W_{[\mathcal{O}]}(c), \quad (5)$$

where each  $c$  represents a non-empty set of  $k$ -spatial indexes. The so called cluster weight  $W_{[\mathcal{O}]}(c)$  contains all terms of the expansion (4), which have at least one power of  $\alpha_k$ ,  $\forall k \in c$ , and no powers of  $\alpha_k$  if  $k \notin c$ . Vice-versa, all terms in Eq. (4) can be included in one of these clusters. Using the inclusion-exclusion principle, one can take  $W_{[\mathcal{O}]}(c)$  out of the sum (5) obtaining the recurrence relation:

$$W_{[\mathcal{O}]}(c) = \mathcal{O}(c) - \sum_{s \subset c} W_{[\mathcal{O}]}(s), \quad (6)$$

where  $\mathcal{O}(c) = \text{Tr}[\hat{\mathcal{O}}\rho_{\text{SS}}(c)]$  is the steady-state expectation value of the observable calculated for the finite cluster  $c$ , the sum runs over all the subclusters  $s$  contained in  $c$ , and  $\rho_{\text{SS}}(c)$  is the steady state of the Liouvillian  $\mathbb{L}(c)$  over the cluster  $c$ . An important property of Eq. (6) is that, if  $c$  is formed out of two disconnected clusters  $c_1$  and  $c_2$ , its weight  $W_{[\mathcal{O}]}(c)$  is zero. This follows from the fact that  $\mathcal{O}$  is an extensive property ( $\mathcal{O}(c) = \mathcal{O}(c_1) + \mathcal{O}(c_2)$ ) and  $c = c_1 + c_2$ .

The symmetries of the Liouvillian  $\mathbb{L}$  may drastically simplify the summation (5), since it is typically not needed to compute all the contributions coming from each cluster. This can be immediately seen, e.g., for situations where the interaction term  $\alpha_k$  between different couples of sites is homogeneous throughout the lattice. In such cases, it is possible to identify the topologically distinct (linked) clusters, so that a representative  $c_n$  for each class can be chosen and counted according to its multiplicity  $\ell(c_n)$  per lattice site (the lattice constant of the graph  $c_n$ ). Here the subscript  $n$  denotes the number of  $k$ -spatial indexes that are grouped in the cluster, that is, its size. The property  $\mathcal{O}$  per lattice site can be thus written directly in the thermodynamic limit  $L \rightarrow \infty$  as:

$$\frac{\mathcal{O}}{L} = \sum_{n=1}^{+\infty} \left[ \sum_{\{c_n\}} \ell(c_n) W_{[\mathcal{O}]}(c_n) \right]. \quad (7)$$

The outer sum runs over all possible cluster sizes, while the inner one accounts for all topologically distinct clusters  $\{c_n\}$  of a given size  $n$ . Let us emphasize that, if the series expansion (7) is truncated up to order  $n = R$ , only clusters  $c$  at most of size  $R$  have to be considered. Indeed each of them should include at least one power of  $\alpha_k$ ,  $\forall k \in c$ . Therefore a cluster of size  $R + 1$  or larger does not contribute to the expansion, up to order  $\alpha^R$ . Moreover the inclusion-exclusion principle guarantees that only connected clusters have a finite weight, and thus contribute to the expansion.

In graph theory, there are established algorithms to compute all topologically distinct clusters, for a given size and lattice geometry. This could drastically increase the efficiency of the NLCE algorithm, since for highly symmetric systems the number of topologically distinct clusters is exponentially smaller than the total number of connected clusters. Explaining how to optimize the cluster generation lies beyond the scope of the present work; however, for the sake of completeness, in App. A we provide details on a basic cluster generation scheme, which has been proposed in Ref. 66. Notice that once all the topologically distinct  $n$ -site clusters and their multiplicities have been generated for a given lattice geometry, one can employ NLCE for any observable and Liouvillian within the same spatial symmetry class of the considered lattice.

A remarkable advantage of NLCE over other numerical methods is that it enables a direct access to the thermodynamic limit, up to order  $R$  in the cluster size, by only counting the cluster contributions of sizes equal or smaller than  $R$  (i.e. using a limited amount of resources). We should stress that, contrary to standard perturbative expansions, there is no perturbative parameter in the system upon which the NLCE is based and can be controlled. Properly speaking, the actual control parameter is given by the amount of correlations that are present in the system: the convergence of the series (7) with  $n$  would be ensured from an order  $R^*$  which is larger than the typical length scale of correlations<sup>61,66</sup>.

In the next sections we give two illustrative examples of how NLCE performs for 2D dissipative quantum lattice models of interacting spin-1/2 particles.

### III. MODEL

Our model of interest is a spin-1/2 lattice system in two dimensions, whose coherent internal dynamics is governed by the anisotropic XYZ-Heisenberg Hamiltonian:

$$\hat{H} = \sum_{\langle i,j \rangle} (J_x \hat{\sigma}_i^x \hat{\sigma}_j^x + J_y \hat{\sigma}_i^y \hat{\sigma}_j^y + J_z \hat{\sigma}_i^z \hat{\sigma}_j^z), \quad (8)$$

where  $\hat{\sigma}_j^\alpha$  ( $\alpha = x, y, z$ ) denote the Pauli matrices for the  $j$ th spin of the system and  $\langle i, j \rangle$  restricts the summation over all couples of nearest neighboring spins. Each spin is subject to an incoherent dissipative process that tends

to flip it down along the  $z$  direction, in an independent way with respect to all the other spins. In the Markovian approximation, such mechanism is faithfully described by the Lindblad jump operator  $\hat{L}_j = \sqrt{\Gamma} \hat{\sigma}_j^-$  acting on each spin:

$$\mathbb{D}[\rho] = \Gamma \sum_j \left[ \hat{\sigma}_j^- \rho \hat{\sigma}_j^+ - \frac{1}{2} \{ \hat{\sigma}_j^+ \hat{\sigma}_j^-, \rho \} \right], \quad (9)$$

where  $\hat{\sigma}_j^\pm = \frac{1}{2} (\hat{\sigma}_j^x \pm i \hat{\sigma}_j^y)$  stands for the corresponding raising and lowering operator along the  $z$  axis, while  $\Gamma$  is the rate of the dissipative processes. in the following we will always work in units of  $\Gamma$ .

The outlined model is particularly relevant as being considered a prototypical dissipative quantum many-body system: its phase diagram is very rich and has been subject to a number of studies at the mean-field level<sup>32</sup> and even beyond such regime, by means of the cluster mean-field<sup>53</sup>, the corner-space renormalization group<sup>39</sup>, and the dissipative PEPS<sup>58</sup>. Remarkably, the Lindblad master equation with the Hamiltonian in Eq. (8) and the dissipator in Eq. (9) presents a  $\mathbb{Z}_2$  symmetry which is associated to a  $\pi$  rotation along the  $z$  axis:  $\hat{\sigma}^x \rightarrow -\hat{\sigma}^x$ ,  $\hat{\sigma}^y \rightarrow -\hat{\sigma}^y$ . For certain values of the couplings  $J_\alpha$ , it is possible to break up this symmetry, thus leading to a dissipative phase transition from a paramagnetic (PM) to a ferromagnetic (FM) phase, the order parameter being the in-plane  $xy$  magnetization. We stress that a XY anisotropy ( $J_x \neq J_y$ ) is necessary to counteract the incoherent spin flips, otherwise the steady-state solution of Eq. (8) would be perfectly polarized, with all the spins pointing down along the  $z$  direction.

The existing literature allows us to benchmark our approach, both far from criticality (Sec. III A) where correlations grow in a controllable way, and in proximity of a  $\mathbb{Z}_2$ -symmetry breaking phase transition (Sec. III B), where correlations diverge in the thermodynamic limit. In the latter we show how it is possible to exploit the NLCE method in combination with a Padé approximants analysis, in order to calculate the location of the critical point as well as the critical exponent  $\gamma$  of the transition, that is associated to a power-law divergence of the magnetic susceptibility to an external field. Contrary to all the other known methods, either being mean-field or dealing with finite-length systems, the NLCE directly addresses the thermodynamic limit and thus, to the best of our knowledge, at present it represents the only unbiased numerical method to calculate such exponent.

### A. Isotropic case

Let us start our analysis by considering a cut in the parameters space which do not cross any critical line. Specifically we set

$$\alpha = J_x = -J_y = J_z. \quad (10)$$

For  $\alpha = 0$  the coherent dynamics is switched off, the coupling in  $x$ - $y$  plane is thus isotropic and the dissipative

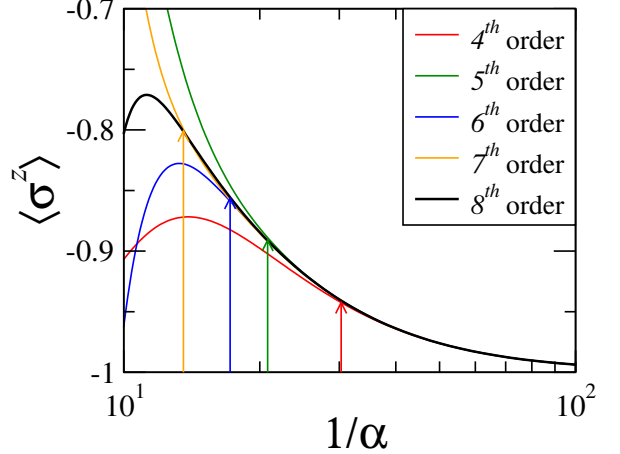


FIG. 1. Steady-state average magnetization along the  $z$  direction for the isotropic Heisenberg model, evaluated by means of the NLCE (bare sum) at different orders  $R$  in the cluster size, as a function of  $1/\alpha$ . The arrows indicate the values of  $\alpha^*$  at which each curve at the  $R$ -th order ( $R < 8$ ) starts deviating significantly from the highest accuracy curve ( $R = 8$ ; thick black line) that we have.

processes cannot be counteracted<sup>32</sup>. As a consequence, regardless of the initial conditions, the steady-state is the pure state having all spins pointing down along the  $z$ -axis:

$$\rho_{\text{ss}}|_{\alpha=0} = \bigotimes_i |\downarrow\rangle\langle\downarrow|. \quad (11)$$

Thus we expect the NLCE would give the exact thermodynamic limit already at first order in the cluster size. As the parameter  $\alpha$  is increased, correlations progressively build up on top of the fully factorizable density matrix (11), therefore higher orders in the expansion of Eq. (7) are needed.

This is exactly what we observe in Fig. 1, where we show the steady-state value of the average magnetization along the  $z$  direction,  $\mathcal{O}/L = \langle \hat{\sigma}_j^z \rangle$ , evaluated by means of the NLCE in Eq (7) up to a given order  $R$ , as function of  $\alpha$ . Note that, as long as  $R$  is increased, the convergence of the NLCE to the most accurate data (highest order that we have) progressively improves. This shows that, in the region where different curves overlap, correlations among the different sites are well captured by the clusters that we are considering in the expansion, up to a given order. When  $\alpha$  is increased the range of correlations grows as well, and one needs to perform the expansion to larger orders. For  $\alpha \gtrsim 0.075$  orders higher than  $R = 8$  are needed to obtain a good convergence in the bare data.

It is however possible to improve the convergence of the expansion without increasing the size of the considered clusters, by simply exploiting two resummation algorithms that have been already shown to be very useful in the context of NLCEs of given thermodynamic properties<sup>61,66</sup>. Specifically we employ the Wynn's algorithm<sup>67</sup> and the Euler transformation<sup>68</sup>, as detailed in App. B.

The results for  $\langle \hat{\sigma}^z \rangle$  as a function of  $\alpha$  are shown in Fig. 2 for various orders in the two resummation schemes (see legends for details). It is immediate to see that the convergence of the expansion is drastically improved of about one order of magnitude. A comparison of NLCEs data with the outcome of simulations obtained by means of quantum trajectories (QT)<sup>69</sup> for finite-size plaquettes shows that the resummed data give qualitatively analogous results up to  $\alpha \approx 1$ , despite a slight discrepancy between them. Such difference is due to the fact that, even if for small  $\alpha$  correlations are very small, finite-system effects are non-negligible: while NLCEs data are directly obtained in the thermodynamic limit, QT are inevitably affected by such effects. As long as  $\alpha$  is decreased, the discrepancy between the two approaches decreases, both leading to  $\langle \hat{\sigma}^z \rangle \rightarrow -1$  in the limit  $\alpha \rightarrow 0$  of Eq. (11).

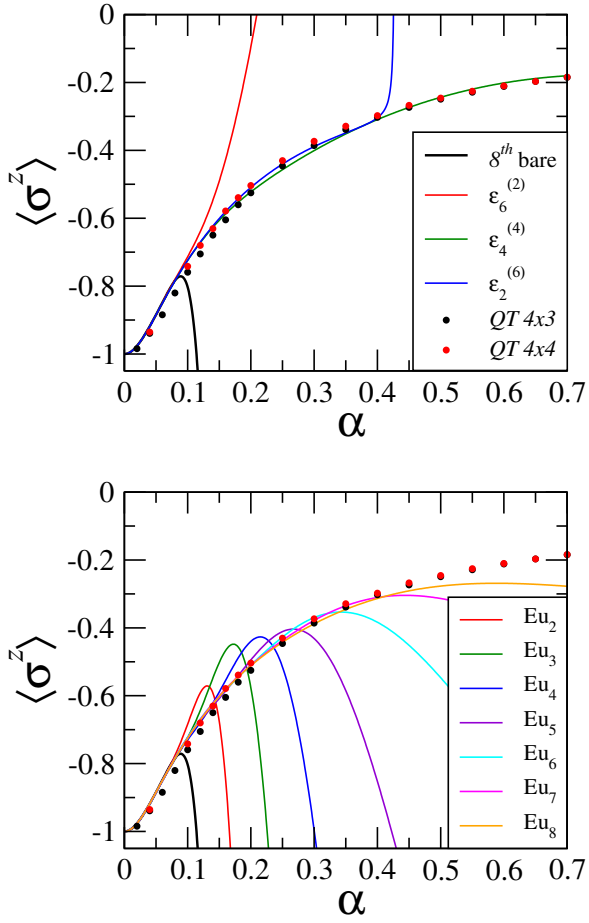


FIG. 2. Steady-state average  $z$ -magnetization as a function of  $\alpha$ , after implementing two resummation techniques on the bare data at order  $R = 8$  (black curve, same as in Fig. 1): Wynn's algorithm (colored curves in the upper panel) and Euler transformation (colored curves in the lower panel). The symbols denote the results of QT simulations for a finite system using periodic boundary conditions, with a  $4 \times 4$  square plaquette (red circles) and a  $4 \times 3$  plaquette (black circles) constructed from the previous one after removing the four sites at the corners.

## B. Anisotropic case and the paramagnetic to ferromagnetic phase transition

We now discuss the more interesting scenario of an anisotropic Heisenberg model ( $J_x \neq J_y \neq J_z$ ), where the system can cross a critical line and exhibit a dissipative phase transition<sup>32</sup>. To this purpose, we set

$$J_x = 0.9, J_y = 0.9 + \alpha, J_z = 1, \quad (12)$$

with  $\alpha \in [0, 0.25]$ . For  $\alpha = 0$  (i.e.,  $J_x = J_y$ ), we come back to the trivial situation where the Hamiltonian conserves the magnetization along the  $z$  direction, and the steady state is the pure state in Eq. (11), with all the spins pointing down in the  $z$  direction. Away from this singular point, for a certain  $\alpha_c > 0$  the system undergoes a second-order phase transition associated to the spontaneous breaking of the  $\mathbb{Z}_2$  symmetry possessed by the master equation (1), from a paramagnetic (PM) for  $\alpha < \alpha_c$ , to a ferromagnetic (FM) phase for  $\alpha > \alpha_c$ . In the FM phase, a finite magnetization in the  $x$ - $y$  plane develops:  $\langle \hat{\sigma}^x \rangle, \langle \hat{\sigma}^y \rangle \neq 0$ , which also defines the order parameter of the transition.

The phenomenology of this phase transition has recently received a lot of attention, and has been investigated at a Gutzwiller mean-field level<sup>32</sup> and by means of more sophisticated methods, including the cluster mean-field approach<sup>53</sup>, the corner-space renormalization technique<sup>39</sup>, and the projected entangled pair operators<sup>58</sup>. The phase transition point for the same choice of parameters of Eq. (12) has been estimated to be  $\alpha_c = 0.1^{32}$ ,  $0.14 \pm 0.01^{53}$  and  $0.17 \pm 0.02^{39}$ .

Here we follow the approach of Rota *et al.*<sup>39</sup> and discuss the magnetic linear response to an applied magnetic field in the  $x$ - $y$  plane, which modifies the Hamiltonian in Eq. (8) according to:

$$\hat{H} \rightarrow \hat{H} + \sum_j h(\hat{\sigma}_j^x \cos \theta + \hat{\sigma}_j^y \sin \theta), \quad (13)$$

where  $\theta$  denotes the field direction,  $[\vec{h}(\theta)] = (h_x, h_y)^T$  and  $h_x = h \cos \theta$ ,  $h_y = h \sin \theta$ . Such response is well captured by the susceptibility tensor  $\chi$ , with matrix elements  $\chi_{\alpha\beta} = \lim_{h_\beta \rightarrow 0} \langle \hat{\sigma}^\alpha \rangle / h_\beta$ . In particular we concentrate on the angularly averaged magnetic susceptibility

$$\chi_{\text{ave}} = \lim_{h \rightarrow 0} \frac{1}{2\pi} \int_0^{2\pi} d\theta \frac{|\vec{M}(\theta)|}{h}, \quad (14)$$

where  $\vec{M}(\theta) = \chi \cdot \vec{h}(\theta)$  is the induced magnetization along an arbitrary direction of the field.

We start by computing the NLCE for the magnetic susceptibility  $\chi_{\text{ave}}$  in the parameter range  $0 \leq \alpha \leq 0.25$ , and improving the convergence of the series up to a given order, by exploiting the Euler algorithm; the latter has been proven to be the most effective for our model of interest. The relevant numerical data are shown in Fig. 3, and are put in direct comparison with those obtained

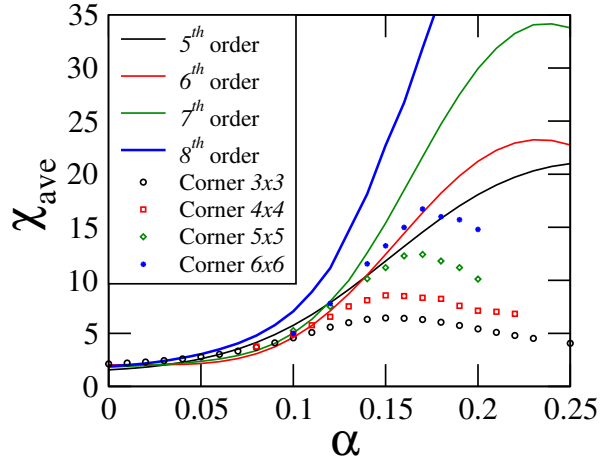


FIG. 3. Angularly averaged magnetic susceptibility to an external field in the  $x$ - $y$  plane, as a function of  $\alpha = J_y - 0.9$ . The continuous curves denote Euler resummed data, to the best achievable expansion, of the bare NLCE results up to the order  $R = 8$ . Symbols are the results from the corner-space renormalization method, taken from Ref. 39.

with an alternative method (the corner-space renormalization group) in Ref. 39. We observe a fairly good agreement with the two approaches, in the small- $\alpha$  parameter range, and point out that in both cases a sudden increase of  $\chi_{\text{ave}}$  for  $\alpha \gtrsim 0.1$  supports the presence of a phase transition in that region. It is however important to remark that, contrary to the isotropic case, here we do not observe an exact data collapse of the NLCEs for  $\chi_{\text{ave}}$ , even for  $\alpha = 0$ . The reason resides in the fact that the presence of an external field (13) makes the structure of the steady state nontrivial, as soon as  $h \neq 0$ , thus admitting correlations to set in.

### 1. Critical behavior

We now show how to exploit the above NLCE data (in combination with a Padé analysis<sup>59</sup>) in order to locate the critical point  $\alpha_c$  for the PM-FM transition, and extract the critical exponent  $\gamma$  of the magnetic susceptibility<sup>70</sup>  $\chi_{\text{ave}} \sim |\alpha - \alpha_c|^{-\gamma}$ . The possibility to extrapolate the critical exponents for a dissipative quantum phase transition is very intriguing, since, to the best of our knowledge, the only numerical work in this context, that is present in the literature, is Ref. 39. However, since finite-size systems are considered there, it was only possible to estimate the finite-size ratio  $\gamma/\nu$ , where  $\nu$  denotes the critical exponent associated to the divergent behavior of the correlation length. The present work offers a complementary point of view since here we are able, for the first time, to provide an independent estimate of the critical exponent  $\gamma$  by directly accessing the thermodynamic limit.

To achieve this goal we study the logarithmic derivative of the averaged magnetic susceptibility, which converts

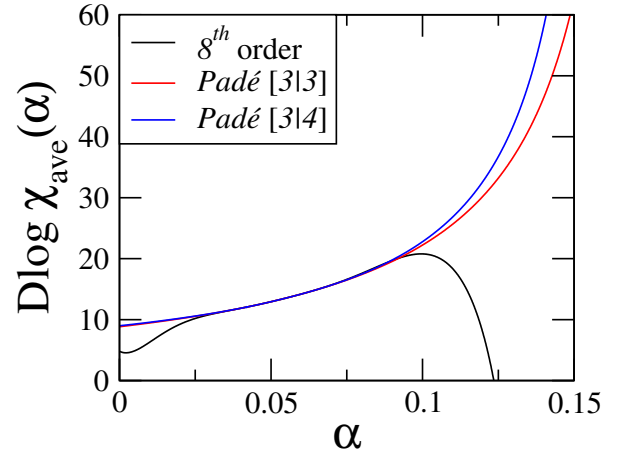


FIG. 4. Logarithmic derivative of  $\chi_{\text{ave}}$  as a function of  $\alpha$ . The black line is obtained from Euler resummed data to the order  $R = 8$  (blue line of Fig. 3). The red and blue lines are the results of the Padé analysis with different [3|3] and [3|4] approximants respectively.

an algebraic singularity into a simple pole<sup>59</sup>:

$$\text{Dlog } \chi_{\text{ave}}(\alpha) \equiv \frac{\chi'_{\text{ave}}(\alpha)}{\chi_{\text{ave}}(\alpha)}. \quad (15)$$

If  $\chi_{\text{ave}} \sim |\alpha - \alpha_c|^{-\gamma}$  for  $|\alpha - \alpha_c| \ll 1$ , the logarithmic derivative behaves as

$$\text{Dlog } \chi_{\text{ave}}(\alpha) \sim \frac{\gamma}{|\alpha - \alpha_c|}. \quad (16)$$

Studying the divergent behavior of Eq. (16) simplifies the problem, since the function  $\text{Dlog } \chi_{\text{ave}}(\alpha)$  has a simple pole at the critical point  $\alpha = \alpha_c$  with a residue corresponding to the critical exponent  $\gamma$ .

In Fig. 4 we show the behavior of the logarithmic derivative calculated from the Euler resummed data to the order  $R = 8$  (blue line in Fig. 3) which represents our best approximation for  $\chi_{\text{ave}}$  at small  $\alpha$ . The behavior at large  $\alpha$  of the function  $\text{Dlog } \chi_{\text{ave}}(\alpha)$  is extrapolated exploiting the Padé approximants. A Padé approximant is a representation of a finite power series as a ratio of two polynomials

$$\text{Dlog } \chi_{\text{ave}}(\alpha) = \sum_{n=0}^R a_n \alpha^n = \frac{P_L(\alpha)}{Q_M(\alpha)}, \quad (17)$$

where  $P_L(\alpha)$  and  $Q_M(\alpha)$  are polynomials of degree  $L$  and  $M$  (with  $L + M \leq R$ ), respectively. This is denoted as the  $[L|M]$  approximant, and can represent functions with simple poles *exactly*. Details about the use of Padé approximants for the study of critical behavior and a discussion about the stability of the method are provided in App. C.

The results of the Padé analysis hint for a divergence at  $\alpha_c = 0.179 \pm 0.001$  with  $\gamma = 1.85 \pm 0.05$  for [3|3], and  $\alpha_c = 0.1665 \pm 0.0005$  with  $\gamma = 1.5 \pm 0.05$  for [3|4]. The

other approximants  $[L|M]$  such that  $L + M \leq R = 8$  do not give physical results in this range of parameters. The error bar is underestimated, since it accounts only for the error introduced in the fitting procedure (see App. C) and neglects the propagation of the numerical error made on the steady-state evaluation. The value of the critical point is in agreement with the results reported in Ref. 53 and Ref. 39, so far.

#### IV. CONCLUSIONS

In this work we have proposed a numerical algorithm based on the generalization of the linked-cluster expansion to open quantum systems on a lattice, allowing to directly access the thermodynamic limit and to evaluate extensive properties of the system. Specifically, we extended the formalism to the Liouvillian case and showed how the basic properties of the expansion are translated to the open-system realm. Given its generality, this method can be applied to open fermionic, bosonic and spin systems in an arbitrary lattice geometry.

We tested our approach with a study of the steady-state properties of the paradigmatic dissipative spin-1/2 XYZ model on a two-dimensional square lattice. Far away from the critical boundaries of the model, we accurately computed the spin magnetization. Upon increasing the order of the expansion, we were able to progressively access regions of the phase diagram that are characterized by a larger amount of correlations among distant sites. The convergence properties of the expansion can be dramatically improved by employing more sophisticated resummation schemes. We then used the numerical linked-cluster expansion across a phase transition in order to study its critical properties. By means of a Padé analysis of the series, we located the critical point and provided the first estimate of the critical exponent  $\gamma$ , which determines the divergent behavior of the (average) magnetic susceptibility close to the phase transition.

At present, this method together with the one in Ref. 58 are the only numerical approaches that allow to compute the steady-state properties of an open lattice model in two spatial dimensions in the thermodynamic limit. Here the intrinsic limitation is that, in order to compute high-order terms in the expansion (and thus to access strongly correlated regions of the phase space), the evaluation of the steady state on a large number of connected sites is required. Furthermore, in the case of bosonic systems, a further complication arises from the local Hilbert space dimension. We believe that a very interesting perspective left for the future, is the combination of the linked-cluster expansion with the corner-space renormalization method<sup>39</sup>, and also possibly with Monte Carlo approaches<sup>71</sup>. Additionally, a careful identification of the internal symmetries of the model may help in decreasing the effective dimension of the Liouvillian space.

#### ACKNOWLEDGMENTS

We thank M. Cè, L. Mazza, and R. Rota for fruitful discussions. We acknowledge the CINECA award under the ISCRA initiative, for the availability of high performance computing resources and support. AB and CC acknowledge support from ERC (via Consolidator Grant CORPHO No. 616233). RF acknowledges support by EU-QUIC, CRF, Singapore Ministry of Education, CPR-QSYNC, SNS-Fondi interni 2014, and the Oxford Martin School. JJ acknowledges support from the National Natural Science Foundation of China No. 11605022, Natural Science Foundation of Liaoning Province No. 2015020110, and the Xinghai Scholar Cultivation Plan and the Fundamental Research Funds for the Central Universities. OV thanks Fundación Rafael del Pino, Fundación Ramón Areces and RCC Harvard.

#### Appendix A: Details on the clusters generation

As mentioned in Sec. II, a careful identification of the symmetries of the Liouvillian allows for a systematic simplification of the expansion in Eq. (7). If a single site is used as the building block for cluster generation (*site expansion*), then the order (the dimension) of a cluster is simply determined by the number of sites that form such cluster.

Here we sketch a simple procedure that can be used to generate and classify all the topologically distinct clusters up to a given order<sup>66</sup>. The algorithm can be summarized as follows: one first generates all linked clusters that can be embedded on the lattice geometry; next, each of them is classified according to its symmetry and topology; finally, the subclusters in each cluster and their multiplicity are evaluated.

For an infinite lattice in the thermodynamic limit, the first step can be carried out (order by order) starting from the smallest possible cluster of one site, and adding up a nearest-neighbor site to every site at the edge of the cluster. Iterating this procedure, from  $n$ -site clusters it is possible to generate clusters with  $n + 1$  sites. In order to obtain all the possible clusters of order  $n + 1$ , one has to perform this operation on all the symmetrically distinct  $n$ -site clusters. This scheme automatically generates only connected clusters, which contribute to the sum in Eq. (7).

Once all the possible  $n$ -site clusters are generated, one has to group them according to their symmetries. For a square lattice geometry (that is the one that we used in the proposed examples) there are eight point group symmetries, provided that the Liouvillian shares the same symmetries of the underlying lattice: identity, rotations by  $m\pi/2$  for  $m = 1, 2, 3$ , reflections about the axes  $x = 0$ ,  $y = 0$ ,  $x = y$ ,  $x = -y$ . Choosing a representative cluster for each symmetrically distinct set, one can compute its multiplicity by applying all the possible symmetry transformations to it, and counting how many dif-

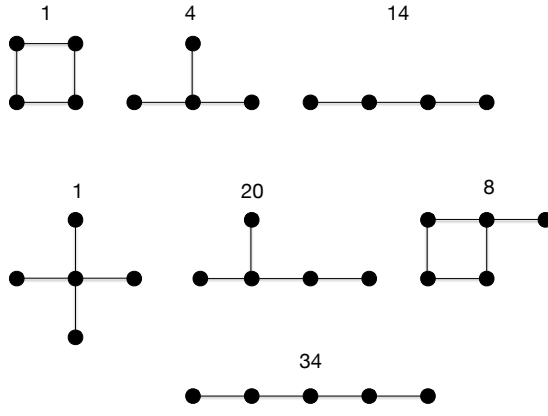


FIG. 5. Topologically distinct clusters in an infinite square lattice, for  $n = 4$  (top line) and  $n = 5$  (bottom lines). The number next to each cluster denotes its multiplicity.

ferent clusters (up to a translation) are found. Next the cluster topology needs to be identified: even if two clusters are not related by any point-group symmetry, they may have exactly the same Hamiltonian, thus being topologically equivalent. In order to check whether two symmetrically distinct  $n$ -site clusters share the same topology one needs to evaluate  $n!$  adjacency matrices (one for each possible site permutation) for one of the two clusters and, compare each of them with the adjacency matrix of the other cluster (without any site permutation). This step is computationally the most demanding. The multiplicity  $\ell(g_n)$  of each topologically distinct cluster  $g_n$  is simply the sum of the multiplicities of the symmetrically distinct clusters with equal topology. In Fig. 5 we sketch the topological clusters and their multiplicities, generated with the procedure outlined above for  $n = 4$  and  $n = 5$ .

The final step involves the identification of subclusters (and their multiplicities) for each topologically distinct cluster. This can be done by repeating the above steps and replacing the infinite square lattice by the topological cluster under consideration. For every generated topological subcluster, one simply compares its adjacency matrix to those of clusters with the same size that have been stored before. This ends up with the construction of a multiplicity matrix  $M_{ij}$  which counts the number of times the  $j$ th topological cluster can be embedded in the  $i$ th topological cluster.

## Appendix B: Resummation algorithms

In order to accelerate the convergence of the series in Eq. (7), some clever resummation techniques can be employed. For the NLCE in equilibrium lattice models, the Wynn's algorithm<sup>67</sup> and Euler transformation<sup>68</sup> have been shown to be particularly useful<sup>66</sup>. In the following

we will briefly review them. We first rewrite Eq. (7) as  $\mathcal{O}/L = \sum_{n=1}^{\infty} S_n$ , where  $S_n = \sum_{\{c_n\}} \ell(c_n) W_{[\mathcal{O}]}(c_n)$  is the partial sum over  $n$ -site clusters. Thus, the expansion to the  $k$ th order read as

$$\frac{\mathcal{O}_k}{L} = \sum_{n=1}^k S_n. \quad (\text{B1})$$

The convergence properties with  $k$  of the NLCE, can be improved by considering different resummation schemes with respect to the bare sum (B1).

### 1. Wynn's algorithm

Let us start by defining

$$\begin{aligned} \varepsilon_n^{(-1)} &= 0, \\ \varepsilon_n^{(0)} &= \mathcal{O}_n, \\ \varepsilon_n^{(k)} &= \varepsilon_{n+1}^{(k-2)} + \frac{1}{\Delta \varepsilon_n^{(k-1)}}, \end{aligned} \quad (\text{B2})$$

with

$$\Delta \varepsilon_n^{(k-1)} = \varepsilon_{n+1}^{(k-1)} - \varepsilon_n^{(k-1)}. \quad (\text{B3})$$

It is expected that the even entries  $\varepsilon_n^{(2l)}$  converge to  $\mathcal{M}/N$ , while the odd ones  $\varepsilon_n^{(2l+1)}$  usually diverge. Here  $l$  defines the number of cycles of improvement. We can arrange all the possible coefficients of Eqs. (B2) in the following matrix  $E_m$ :

$$E_m = \begin{pmatrix} \varepsilon_1^{(1)} & \varepsilon_2^{(1)} & \dots & \varepsilon_{m-2}^{(1)} & \varepsilon_{m-1}^{(1)} \\ \varepsilon_1^{(2)} & \varepsilon_2^{(2)} & \dots & \varepsilon_{m-2}^{(2)} & 0 \\ \vdots & \vdots & \dots & 0 & 0 \\ \varepsilon_1^{(m-2)} & \varepsilon_2^{(m-2)} & 0 & 0 & \dots \\ \varepsilon_1^{(m-1)} & 0 & 0 & \dots & \dots \end{pmatrix}, \quad (\text{B4})$$

where  $m$  is the cut-off order of the bare sums. The entries needed in the  $l$ th cycles of improvement are the non-zero elements in the  $(m-2l)$ th and  $(m-2l+1)$ th columns of  $E_m$ .

As an example, let us suppose to use the Wynn's algorithm with  $l = 1$  instead of the bare sum

$$\begin{aligned} \mathcal{O}_m \rightarrow \varepsilon_{m-2}^{(2)} &= \varepsilon_{m-1}^{(0)} - \frac{1}{\varepsilon_{m-1}^{(1)} - \varepsilon_{m-2}^{(2)}} \\ &= \mathcal{O}_m - \frac{S_m}{1 - S_{m-1}/S_m}, \end{aligned} \quad (\text{B5})$$

from which we see that the last term on the r.h.s. of the second line is the first order correction of  $\mathcal{O}_m$ . Note that, for every cycle of improvement, there are two terms less in the new series generated by means of Eq. (B2) ( $\mathcal{O}_m \rightarrow \varepsilon_{m-2l}^{(2l)}$ ).

## 2. Euler transformation

The Euler transformation turns out to be very useful for the series in which  $S_n$  is alternating in sign. Within this method, the partial sum  $S_n$  is replaced by  $u_n = (-1)^n S_n$ . The observable  $\mathcal{O}/N$  is computed approximately by the following formula, with  $m$  being the cut-off order of the bare sum:

$$\frac{\mathcal{O}}{N} \approx u_0 - u_1 + u_2 - \cdots - u_{n-1} + \sum_{l=0}^{m-n} \frac{(-1)^l}{2^{l+1}} \Delta^l u_n, \quad (\text{B6})$$

where  $\Delta$  defines the forward differentiating operator, as

$$\begin{aligned} \Delta^0 u_n &= u_n, \\ \Delta^1 u_n &= u_{n+1} - u_n, \\ \Delta^2 u_n &= u_{n+2} - 2u_{n+1} + u_n, \\ \Delta^3 u_n &= u_{n+3} - 3u_{n+2} + 3u_{n+1} - u_n, \end{aligned} \quad (\text{B7})$$

and so on, while  $n-1$  is the number of terms for which the bare sum is performed before the Euler transformation is implemented. The first few terms of the approximation can be written as

$$\mathcal{O}_m \rightarrow \mathcal{O}_{n-1} + (-1)^n \left[ \frac{S_n}{2} + \frac{S_n + S_{n+1}}{4} + \cdots \right]. \quad (\text{B8})$$

For further details about the Euler transformation see also Refs. 68 and 72.

## Appendix C: Padé approximants

Here we discuss the details related to the Padé analysis of the divergent behavior of the magnetic susceptibility, which has been performed in Sec. III B 1. As already introduced in the main text, the Padé approximant is a representation of the first  $N$  terms of a power series as a ratio of two polynomials. Here, for the sake of clarity, we recall the main definitions.

Let us suppose that  $f(\alpha)$  is the function under consideration and that we know its Taylor expansion up to the  $R$ -th order. Thus

$$f(\alpha) = \sum_{n=0}^R a_n \alpha^n = \frac{P_L(\alpha)}{Q_M(\alpha)}, \quad (\text{C1})$$

where

$$P_L(\alpha) = \sum_{n=0}^L p_n \alpha^n, \quad Q_M(\alpha) = 1 + \sum_{n=1}^M q_n \alpha^n, \quad (\text{C2})$$

and  $L + M \leq R$ . This is denoted as the  $[L|M]$  approximant. A Padé approximant can represent exactly functions with simple poles. So that, instead of studying the

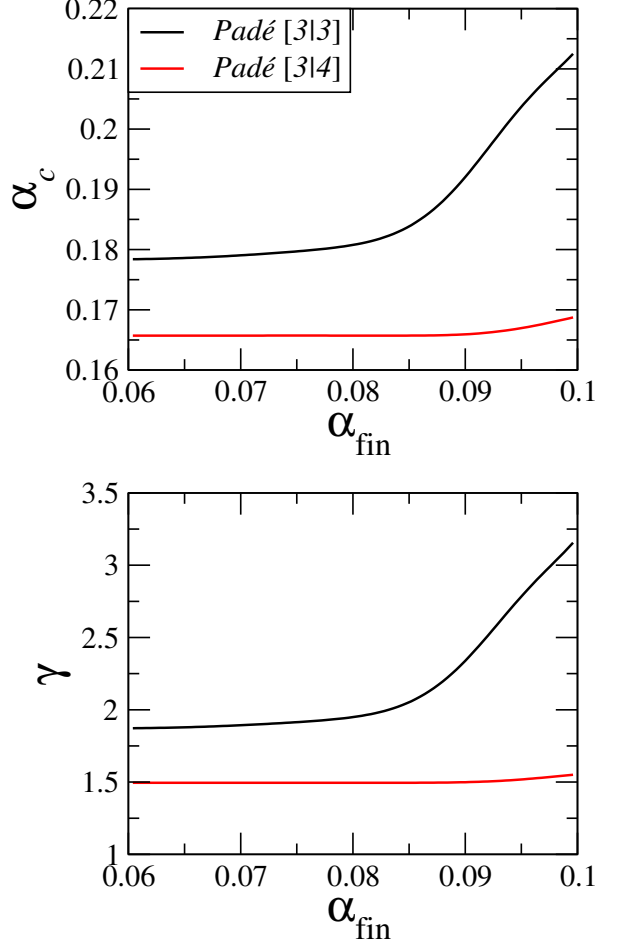


FIG. 6. Position of the critical point  $\alpha_c$  (top panel) and value of the critical exponent  $\gamma$  (bottom panel) as a function of the upper boundary of the fitting region  $\alpha_{\text{fin}}$

critical behavior of  $\chi_{\text{ave}}$  [see Eq. (14)] we analyze its logarithmic derivative

$$\text{Dlog } \chi_{\text{ave}}(\alpha) = \frac{\chi'_{\text{ave}}(\alpha)}{\chi_{\text{ave}}(\alpha)}, \quad (\text{C3})$$

which has a simple pole  $\alpha = \alpha_c$  with residue  $-\gamma$ . To show this, let us note that for  $|\alpha - \alpha_c| \ll 1$

$$\chi_{\text{ave}}(\alpha) = \frac{g(\alpha)}{|\alpha - \alpha_c|^\gamma}, \quad (\text{C4})$$

where  $g(\alpha)$  is an analytic function in the range of  $\alpha$  we are interested in. So that Eq. (C4) becomes

$$\text{Dlog } \chi_{\text{ave}}(\alpha) = \frac{g'(\alpha)}{g(\alpha)} - \frac{\gamma}{|\alpha - \alpha_c|}. \quad (\text{C5})$$

Our best approximation of the function  $\text{Dlog } \chi_{\text{ave}}(\alpha)$  is obtained by fitting (with an 8-th degree polynomial) the Euler resummed data for  $R = 8$  (blue line in Fig. 3) for  $0 \leq \alpha \leq 0.1$  and then computing analytically Eq. (C3). The other parameters are set as in Eq. (12). Next, we fit

$\text{Dlog } \chi_{\text{ave}}(\alpha)$  (with an 8-th degree polynomial) between  $\alpha_{\text{in}} = 0.05$  to  $0.06 \leq \alpha_{\text{fin}} \leq 0.1$  in order to obtain the coefficients  $\{a_n \mid n = 1, \dots, R = 8\}$ . Given the  $\{a_n\}$ , it is easy to evaluate the coefficients  $\{p_n\}$  and  $\{q_n\}$  in Eq. (C2) exploiting Eq. (C1). This give the following set of linear equations

$$\begin{aligned}
 a_0 &= p_0 \\
 a_1 + a_0 q_1 &= p_1 \\
 a_2 + a_1 q_1 + a_0 q_2 &= p_2 \\
 &\vdots \\
 a_L + a_{L-1} q_1 + \dots + a_0 q_L &= p_L \\
 a_{L+1} + a_L q_1 + \dots + a_{L-M+1} q_M &= 0 \\
 &\vdots \\
 a_{L+M} + a_{L+M-1} q_1 + \dots + a_L q_M &= 0. \tag{C6}
 \end{aligned}$$

Once the system (C6) is solved, one can find the position of the (simple) pole  $\alpha_c$  by evaluating the zeroes of  $Q_M$ . Typically, only one of the  $M$  zeroes is real and located in the region of interest. The critical exponent is then evaluated by computing the residue of  $Q_M(\alpha)$  at  $\alpha = \alpha_c$ :

$$\gamma = - \lim_{\alpha \rightarrow \alpha_c} Q_M(\alpha)(\alpha - \alpha_c). \tag{C7}$$

In Fig. 6 we show the position of the critical point  $\alpha_c$  (top panel) and value of critical exponent  $\gamma$  (bottom panel) as a function of the upper fit boundary  $\alpha_{\text{fin}}$ . We note that the Padé analysis gives stable results for  $0.06 \leq \alpha_{\text{fin}} \leq 0.08$  and  $0.06 \leq \alpha_{\text{fin}} \leq 0.095$  for the approximants [3|3] and [3|4] respectively. In this fitting range we get  $\alpha_c = 0.179 \pm 0.001$  with  $\gamma = 1.85 \pm 0.05$  for [3|3], and  $\alpha_c = 0.1665 \pm 0.0005$  and  $\gamma = 1.5 \pm 0.05$  for [3|4]. The other approximants  $[L|M]$  such that  $L + M \leq R = 8$  do not give physical results in this range of parameters.

---

<sup>1</sup> J. Kasprzak, M. Richard, S. Kundermann, A. Baas, P. Jeambrun, J. M. J. Keeling, F. M. Marchetti, M. H. Szymanska, R. André, J. L. Staehli, V. Savona, P. B. Littlewood, B. Deveaud, and Le Si Dang, *Nature* **443**, 409 (2006).

<sup>2</sup> N. Syassen, D. M. Bauer, M. Lettner, T. Volz, D. Dietze, J. J. García-Ripoll, J. I. Cirac, G. Rempe, and S. Dürr, *Science* **320**, 1329 (2008).

<sup>3</sup> K. Baumann, C. Guerlin, F. Brennecke, and T. Esslinger, *Nature* **464**, 1301 (2010).

<sup>4</sup> M. Müller, S. Diehl, G. Pupillo, and P. Zoller, *Adv. At. Mol. Opt. Phys.* **61**, 1 (2012).

<sup>5</sup> A. A. Houck, H. E. Türeci, and J. Koch, *Nat. Phys.* **8**, 292 (2012).

<sup>6</sup> M. Ludwig and F. Marquardt, *Phys. Rev. Lett.* **111**, 073603 (2013).

<sup>7</sup> A. Tomadin and R. Fazio, *J. Opt. Soc. Am. B* **27**, A130 (2010).

<sup>8</sup> M. Hartmann, *J. Opt.* **18**, 104005 (2016).

<sup>9</sup> L. M. Sieberer, M. Buchhold, and S. Diehl, *Rep. Prog. Phys.* **79**, 096001 (2016).

<sup>10</sup> K. Le Hur, L. Henriet, A. Petrescu, K. Plekhanov, G. Roux, and M. Schiró, *C. R. Physique* **17**, 808 (2016).

<sup>11</sup> C. Noh and D. Angelakis, *Rep. Prog. Phys.* **80**, 016401 (2017).

<sup>12</sup> A. Tomadin, V. Giovannetti, R. Fazio, D. Gerace, I. Carusotto, H. E. Türeci, and A. Imamoglu, *Phys. Rev. A* **81**, 061801 (2010).

<sup>13</sup> I. Carusotto, D. Gerace, H. E. Türeci, S. De Liberato, C. Ciuti, and A. Imamoglu, *Phys. Rev. Lett.* **103**, 033601 (2009).

<sup>14</sup> T. Grujic, S. R. Clark, D. G. Angelakis, and D. Jaksch, *New J. Phys.* **14**, 103025 (2012); T. Grujic, S. R. Clark, D. Jaksch, and D. G. Angelakis, *Phys. Rev. A* **87**, 053846 (2013).

<sup>15</sup> J. Ruiz-Rivas, E. del Valle, C. Gies, P. Gartner, and M. J. Hartmann, *Phys. Rev. A* **90**, 033808 (2014).

<sup>16</sup> A. Biella, L. Mazza, I. Carusotto, D. Rossini, and R. Fazio, *Phys. Rev. A* **91**, 053815 (2015).

<sup>17</sup> C. Lee, C. Noh, N. Schetakis, and D. G. Angelakis, *Phys. Rev. A* **92**, 063817 (2015).

<sup>18</sup> T. Mertz, I. Vasić, M. J. Hartmann, and W. Hofstetter, *Phys. Rev. A* **94**, 013809 (2016).

<sup>19</sup> K. Debnath, E. Mascarenhas, V. Savona, arXiv:1706.04936 (2017).

<sup>20</sup> J. Reisons, E. Mascarenhas, V. Savona, arXiv:1706.08272 (2017).

<sup>21</sup> S. Diehl, A. Micheli, A. Kantian, B. Kraus, H. P. Büchler, and P. Zoller, *Nat. Phys.* **4**, 878 (2008).

<sup>22</sup> F. Verstraete, M. M. Wolf, and J. I. Cirac, *Nat. Phys.* **5**, 633 (2009).

<sup>23</sup> M. J. Hartmann, *Phys. Rev. Lett.* **104**, 113601 (2010).

<sup>24</sup> R. O. Umucalilar and I. Carusotto, *Phys. Rev. Lett.* **108**, 206809 (2012).

<sup>25</sup> J. Jin, D. Rossini, R. Fazio, M. Leib, and M. J. Hartmann, *Phys. Rev. Lett.* **110**, 163605 (2013). J. Jin, D. Rossini, M. Leib, M. J. Hartmann, and R. Fazio, *Phys. Rev. A* **90**, 023827 (2014).

<sup>26</sup> T. Yuge, K. Kamide, M. Yamaguchi, and T. Ogawa, *J. Phys. Soc. Jpn.* **83**, 123001 (2014).

<sup>27</sup> M. Hoenig, W. Abdussalam, M. Fleischhauer, and T. Pohl, *Phys. Rev. A* **90**, 021603(R) (2014).

<sup>28</sup> C.-K. Chan, T. E. Lee, and S. Gopalakrishnan, *Phys. Rev. A* **91**, 051601 (2015).

<sup>29</sup> R. M. Wilson, W. K. Mahmud, A. Hu, A. V. Gorshkov, M. Hafezi, and M. Foss-Feig, *Phys. Rev. A* **94**, 033801 (2016).

<sup>30</sup> M. Foss-Feig, P. Niroula, J. T. Young, M. Hafezi, A. V. Gorshkov, R. M. Wilson, and M. F. Maghrebi, *Phys. Rev. A* **95**, 043826 (2017).

<sup>31</sup> T. E. Lee, H. Häffner, and M. C. Cross, *Phys. Rev. A* **84**, 031402 (2011).

<sup>32</sup> T. E. Lee, S. Gopalakrishnan, and M. D. Lukin, *Phys. Rev. Lett.* **110**, 257204 (2013).

<sup>33</sup> V. Savona, arXiv:1705.02865.

<sup>34</sup> J. Lebreuilly, A. Biella, F. Storme, D. Rossini, R. Fazio, C. Ciuti, I. Carusotto, arXiv:1704.01106 (2017).

<sup>35</sup> A. Biella, F. Storme, J. Lebreuilly, D. Rossini, R. Fazio, I. Carusotto, C. Ciuti, *Phys. Rev. A* **96**, 023839 (2017).

<sup>36</sup> E. G. Dalla Torre, E. Demler, T. Giamarchi, and E. Altman, Phys. Rev. B **85**, 184302 (2012).

<sup>37</sup> L. M. Sieberer, S. D. Huber, E. Altman, and S. Diehl, Phys. Rev. Lett. **110**, 195301 (2013).

<sup>38</sup> J. Marino and S. Diehl, Phys. Rev. Lett. **116**, 070407 (2016).

<sup>39</sup> R. Rota, F. Storme, N. Bartolo, R. Fazio, and C. Ciuti, Phys. Rev. B **95**, 134431 (2017).

<sup>40</sup> M. Fitzpatrick, N. M. Sundaresan, A. C. Y. Li, J. Koch, and A. A. Houck, Phys. Rev. X **7**, 011016 (2017).

<sup>41</sup> H.-P. Breuer and F. Petruccione, *The Theory of Open Quantum Systems* (Oxford University Press, New York, 2002).

<sup>42</sup> A. Rivas and S. F. Huelga, *Open Quantum Systems. An Introduction* (Springer, Heidelberg, 2011).

<sup>43</sup> V. V. Albert and L. Jiang, Phys. Rev. A **89**, 022118 (2014).

<sup>44</sup> T. Prosen, New J. Phys. **10**, 043026 (2008).

<sup>45</sup> A. C. Y. Li, F. Petruccione, and J. Koch, Sci. Rep. **4**, 4887 (2014); Phys. Rev. X **6**, 021037 (2016).

<sup>46</sup> M. F. Maghrebi and A. V. Gorshkov, Phys. Rev. B **93**, 014307 (2016).

<sup>47</sup> F. Verstraete, J. J. García-Ripoll, and J. I. Cirac, Phys. Rev. Lett. **93**, 207204 (2004).

<sup>48</sup> M. Zwolak and G. Vidal, Phys. Rev. Lett. **93**, 207205 (2004).

<sup>49</sup> T. Prosen and M. Znidaric, J. Stat. Mech. (2009) P02035.

<sup>50</sup> J. Cui, J. I. Cirac, and M. C. Bañuls, Phys. Rev. Lett. **114**, 220601 (2015).

<sup>51</sup> E. Mascarenhas, H. Flayac, and V. Savona, Phys. Rev. A **92**, 022116 (2015).

<sup>52</sup> A. H. Werner, D. Jaschke, P. Silvi, M. Kliesch, T. Calarco, J. Eisert, and S. Montangero, Phys. Rev. Lett. **116**, 237201 (2016).

<sup>53</sup> J. Jin, A. Biella, O Viyuela, L. Mazza, J. Keeling, R. Fazio, and D. Rossini, Phys. Rev. X **6**, 031011 (2016).

<sup>54</sup> P. Degenfeld-Schonburg and M. J. Hartmann, Phys. Rev. B **89**, 245108 (2014).

<sup>55</sup> H. Weimer, Phys. Rev. Lett. **114**, 040402 (2015).

<sup>56</sup> W. Casteels, S. Finazzi, A. Le Boit  , F. Storme, and C. Ciuti, New J. Phys. **18**, 093007 (2016).

<sup>57</sup> S. Finazzi, A. Le Boit  , F. Storme, A. Baksic, and C. Ciuti, Phys. Rev. Lett. **115**, 080604 (2015).

<sup>58</sup> A. Kshetrimayum, H. Weimer, and R. Orus, arXiv:1612.00656 (2016).

<sup>59</sup> J. Oitmaa, C. Hamer, and W. Zheng, *Series expansion methods for strongly interacting lattice models*, (Cambridge University Press, Cambridge, 2006).

<sup>60</sup> C. N. Yang and T. D. Lee, Phys. Rev. **87**, 404 (1952); *ibid.* **87**, 410 (1952).

<sup>61</sup> M. Rigol, T. Bryant, and R. R. P. Singh, Phys. Rev. Lett. **97**, 187202 (2006).

<sup>62</sup> M. Rigol, T. Bryant, and R. R. P. Singh, Phys. Rev. E **75**, 061118 (2007); *ibid.* **75**, 061119 (2007).

<sup>63</sup> M. Rigol, Phys. Rev. Lett. **112**, 170601 (2014).

<sup>64</sup> K. Mallayya and M. Rigol, Phys. Rev. E **95**, 033302 (2017).

<sup>65</sup> B. Bruognolo, Z. Zhu, S. R. White, and E. M. Stoudenmire, arXiv:1705.05578 (2017).

<sup>66</sup> B. Tang, E. Khatami, and M. Rigol, Comp. Phys. Commun. **184**, 557 (2013).

<sup>67</sup> A. J. Guttmann, *Phase Transitions and Critical Phenomena*, Vol.13 (Academic Press, London, 1989).

<sup>68</sup> H. W. Press, B. P. Flannery, S. A. Teukolsky, and W. T. Vetterling, *Numerical Recipes in Fortran* (Cambridge University Press, Cambridge, England, 1999).

<sup>69</sup> J. Dalibard, Y. Castin, and K. M  lmer, Phys. Rev. Lett. **68**, 580 (1992).

<sup>70</sup> S. Sachdev, *Quantum Phase Transitions* (Cambridge University Press, Cambridge, England, 2000).

<sup>71</sup> A. Nagy and V. Savona, private communication.

<sup>72</sup> K. Knopp, *Theory and Application of Infinite Series* (Dover Publications, New York, 1990).